JOURNAL OF GEOPHYSICAL RESEARCH, VOL. 101, NO. D6, PAGES 9757–9773, APRIL 30, 1996

Validation studies using multiwavelength Cryogenic Limb Array Etalon Spectrometer (CLAES) observations of stratospheric aerosol

Steven T. Massie,[1] John C. Gille,[1] David P. Edwards,[1] Paul L. Bailey,[1] Lawrence V. Lyjak,[1] Cheryl A. Craig,[1] Charles P. Cavanaugh,[1] John L. Mergenthaler,[2] Aidan E. Roche,[2] John B. Kumer,[2] Alyn Lambert,[3] Roy G. Grainger,[3] Clive D. Rodgers,[3] Frederic W. Taylor,[3] James M. Russell III,[4] Jae H. Park,[4] Terry Deshler,[5] Mark. E. Hervig,[5] Evan F. Fishbein,[6] Joe W. Waters,[6] and William A. Lahoz[7]

Abstract. Validation studies of multiwavelength Cryogenic Limb Array Etalon Spectrometer (CLAES) observations of stratospheric aerosol are discussed. An error analysis of the CLAES aerosol extinction data is presented. Aerosol extinction precision values are estimated at latitudes and times at which consecutive Upper Atmosphere Research Satellite (UARS) orbits overlap. Comparisons of CLAES aerosol data with theoretical Mie calculations, based upon in situ particle size measurements at Laramie, Wyoming, are presented. CLAES aerosol data are also compared to scaled aerosol extinction measured by the Stratospheric Acrosol and Gas Experiment (SAGE II) and Atmospheric Trace Molecule Spectroscopy (ATMOS) experiments. Observed and calculated extinction spectra, from CLAES, Improved Stratospheric and Mesospheric Sounder (ISAMS), and Halogen Occultation Experiment (HALOE) data, are compared. CLAES extinction data have precisions between 10 and 25%, instrumental biases near 30%, and accuracies between 33 and 43%.

1. Introduction

This paper discusses validation studies using the first public release (version 7) aerosol measurements from the Cryogenic Limb Array Etalon Spectrometer (CLAES) experiment of the Upper Atmosphere Research Satellite (UARS). Validation studies of CLAES aerosol data are of interest for several reasons. It is important to understand the quantitative contribution of aerosols to the radiance profiles observed by CLAES. Mount Pinatubo erupted in June 1991, 3 months before the launch of UARS in September 1991, and as discussed below, stratospheric aerosol made an important contribution to the observed radiance profiles, at altitudes below 30 km. It is also important to know the precision and accuracy of the CLAES aerosol data before it is used in quantitative studies. Theoretical studies which use global distributions of aerosol to test dynamical models of stratospheric circulation and theoretical studies which address issues of heterogeneous chemistry at midlatitudes and in the polar regions require estimates of precision and accuracy of the aerosol data before a meaningful comparison between theory and observation can be made.

[1]National Center for Atmospheric Research, Boulder, Colorado.
[2]Lockheed Palo Alto Research Laboratory, Palo Alto, California.
[3]Atmospheric, Oceanic and Planetary Physics, University of Oxford, Oxford, United Kingdom.
[4]NASA Langley Research Center, Hampton, Virginia.
[5]University of Wyoming, Laramie, Wyoming.
[6]Jet Propulsion Laboratory, California Institute of Technology, Pasadena, California.
[7]University of Reading, Reading, United Kingdom.

Paper number 95JD03225.
0148-0227/96/95JD-03225$05.00

While this paper focuses upon CLAES data, several other instruments on UARS also measure stratospheric aerosol, and one instrument measures gaseous SO_2. Validation studies, similar to that of CLAES, are discussed in several papers in this special *Journal of Geophysical Research* UARS validation issue. Discussions of UARS data, in general, are given elsewhere. CLAES observations of stratospheric aerosol are discussed in several papers [*Mergenthaler et al.*, 1993; *Roche et al.*, 1994; *Massie et al.*,1994]. The Microwave Limb Sounder (MLS) measures SO_2, the precursor gas which is transformed into sulfate aerosol after volcanic eruptions [*Read et al.*, 1993]. The Improved Stratospheric and Mesospheric Sounder (ISAMS) observes aerosol extinction at 12.11 and 6.20 μm [*Lambert et al.*, 1993; *Grainger et al.*, 1993]. The Halogen Occultation Experiment (HALOE) observes aerosol extinction at 2.45, 3.40, 3.46, and 5.26 μm [*Hervig et al.*, 1993]. Aerosol scattering is observed by the High-Resolution Doppler Imager (HRDI) at 630 and 690 nm [*Hays et al.*, 1993].

To facilitate comparisons with the aerosol data of other aerosol measuring systems, UARS aerosol data are reported in reciprocal length units. The CLAES, ISAMS, and HALOE experiments report extinction values in km^{-1} units, and the HRDI experiment reports extinction in m^{-1} units. These units are common to lidar and other satellite systems, such as the Stratospheric Aerosol and Gas Experiment (SAGE I and II) and the Stratospheric Aerosol Measurement (SAM II) satellite experiments [*World Meteorological Organization* (WMO), 1991; *McCormick and Vega*, 1992; *McCormick et al.*, 1989; *Poole and Pitts*, 1994].

This validation paper proceeds in the following manner: A discussion of the CLAES experiment and an error analysis, similar to those carried out in companion papers on validation of CLAES temperature [*Gille et al.*, this issue], HNO_3 [*Kumer et al.*, this issue], CH_4 and N_2O [*Roche et al.*, this issue], and $ClONO_2$ data [*Mergenthaler et al.*, this issue], are presented. This paper also

presents estimates of the precision of CLAES extinction values for eight of its filter band passes, determined as a function of pressure level, for the time periods between January 1992 and April 1993 (CLAES exhausted its supply of cryogen in May 1993). The CLAES aerosol extinction precision values are estimated at latitudes and times at which consecutive UARS orbits overlap.

CLAES extinction data are then compared with several different types of correlative measurements. Particle size distribution measurements, obtained over Laramie, Wyoming, are used in Mie calculations to predict infrared extinction altitude profiles, which are compared to the CLAES data. Another source of correlative data is that of the SAGE II and ATMOS experiments. SAGE II extinction profiles at 0.525 μm are multiplied by Mie theoretical scaling factors to derive extinction profiles at the CLAES wavelengths, and these data are compared to the CLAES data. ATMOS aerosol spectra are also compared to coincident CLAES aerosol extinction measurements. Using other UARS aerosol data sets, percent differences between ISAMS and CLAES data are calculated for the January 1992 and April 1992 time periods, as a function of pressure level and latitude. These comparisons check the consistency of the CLAES and ISAMS data on a global basis. Finally, multiwavelength coadded spectra from each of the CLAES, ISAMS, and HALOE instruments are compared to theoretical spectra for sulfate aerosol particles.

2. CLAES Experiment

The CLAES optical system, measurement technique, and modes of operation are described by *Roche et al.* [1993]. While viewing the atmosphere, CLAES operated mostly in a nominal science mode. In this mode, for each of nine blocker filters, a Fabry-Perot etalon was driven sequentially to a set of etalon tilt angles that provided approximately 0.25 cm^{-1} resolution in a predetermined set of spectral channels, selected to optimize information content for retrieval purposes. Data were obtained (with a repeat cycle of 65 s) at altitudes typically between 10 and 60 km by an array of 20 solid state detectors, with a vertical resolution of 2.5 km. Retrieval software then obtains altitude profiles of temperature, mixing ratio profiles of O_3, H_2O, HNO_3, N_2O, CH_4, CFC-12, CFC-11, $ClONO_2$, N_2O_5, NO_2, and NO, and km^{-1} profiles of aerosol.

The blocker regions for which aerosol profiles are retrieved are given in Table 1. Each blocker region has between four and nine spectral channels. Some of these channels include the line centers of species to be retrieved, and some channels are located between lines, in order to simultaneously retrieve aerosol, or other continuum features.

The simultaneous retrieval of pressure (hPa) and temperature (K), gaseous constituents (mixing ratios), and the total continua (expressed as an extinction coefficient, in km^{-1}), is discussed by *Kumer et al.* [this issue]. A linear least squares approach for fitting calculated radiances to the observed data is used to translate the CLAES multiemitter multichannel problem into one in which there is a single emitter and single channel for each species. Using blocker 8 (centered near 790 cm^{-1}, 12.65 μm) as an example, the retrieval of temperature, O_3, and aerosol is performed using a method similar to the Newtonian iterative algorithm [see *Rodgers*, 1975, equation (99), p. 621]. For production data processing, the method requires a computationally efficient algorithm for calculation of radiance profiles. The model described by *Marshall et al.* [1994] is used for this purpose. In other CLAES blocker regions the same approach is applied for species and aerosol retrieval. The CLAES production software produces, in this way, an independent aerosol retrieval in each of the blocker regions listed in Table 1.

Table 1. Wavelengths for Each CLAES Blocker Filter Region

Blocker	Wavelength, μm	Wavenumber, cm^{-1}
9	12.82	780
8	12.65	790
7	11.90	840
6	11.36	880
5	10.83	925
4	7.95	1257
3	6.23	1605

CLAES, Cryogenic Limb Array Etalon Spectrometer.

The continuum extinction observed by CLAES is due to aerosol and cloud opacity, the contributions of minor gases which are not retrieved in the operational software, and at 6.23 μm also due to the pressure-induced absorption (PIA) of molecular oxygen. In the 6.23-μm (1605 cm^{-1}) blocker region the extinction coefficient is equal to the sum of all of the radiative sources cited above. Correlative studies presented here use the extinction corrected by subtracting off the PIA component. Table 2 lists the values of the PIA correction, as a function of temperature and pressure, for the 6.23-μm blocker region. The PIA values are derived from the laboratory measurements of *Orlando et al.* [1991]. Note that the PIA correction to the data is substantial and has a pressure-squared dependence. At 20 km altitude, at midlatitudes, the correction is typically 33% of the total extinction coefficient. At 20 km altitude, in the polar regions, the correction is roughly 40% of the total extinction coefficient.

For the blocker 4 data near 7.95 μm (1257 cm^{-1}), aerosol and N_2O_5 both have wavelength dependencies which are fairly flat across the 10 cm^{-1} blocker filter band pass. In the version 7 processing the continuum emission is assumed to be due to aerosol extinction for altitudes below the altitude level at which the continuum emission has an extinction coefficient equal to 6.3×10^{-5} km^{-1}. For altitudes above this threshold value, the continuum emission is assumed to be due to N_2O_5. At these higher altitudes the aerosol extinction is modeled by a smooth decrease with altitude. The quality indicators associated with the aerosol extinction indicates that this model is used. The value of 6.3×10^{-5} km^{-1} was chosen by noting empirically where diurnal dependence

Table 2. Pressure induced absorption (PIA) data (1.0×10^{-4} km^{-1})

	Pressure, hPa					
Temperature, K	10	21	31	46	68	100
180	0.255	1.13	2.45	5.40	11.8	25.5
200	0.180	0.795	1.73	3.81	8.33	18.0
220	0.132	0.581	1.27	2.79	6.10	13.2
240	0.100	0.442	0.964	2.12	4.64	10.0
260	0.079	0.350	0.762	1.68	3.67	7.93
280	0.065	0.287	0.626	1.38	3.01	6.52

Values are derived from the laboratory study of *Orlando et al.* [1991].

Table 3. Model N_2O_5 continuum data (1.0×10^{-4} km^{-1})

Temperature, K	Pressure, hPa					
	10	21	31	46	68	100
180	0.576	0.440	0.324	0.241	0.178	0.157
200	0.518	0.396	0.292	0.217	0.160	0.141
220	0.471	0.360	0.265	0.197	0.146	0.128
240	0.432	0.330	0.243	0.181	0.133	0.118
260	0.399	0.304	0.225	0.167	0.123	0.109
280	0.370	0.283	0.209	0.155	0.114	0.101

Values are derived from the laboratory study of *Cantrell et al.* [1988], and midlatitude N_2O_5 mixing ratios (1.1, 0.4, 0.2, 0.1, 0.05, and 0.03 ppbv at 10, 21, 31, 46, 68, and 100 hPa).

in the atmospheric emission was present in previous developmental retrievals of the aerosol. The 7.96-μm aerosol extinction values, in this paper, are corrected by the model values listed in Table 3, which are based upon a midlatitude N_2O_5 mixing ratio profile, and the *Cantrell et al.* [1988] N_2O_5 temperature-dependent cross sections. At 20 km the N_2O_5 correction is small and is of the order of 2%. The N_2O_5 correction becomes larger than the aerosol extinction between 25 and 35 km altitude, at an altitude dependent upon the aerosol extinction altitude profile. This version 7 processing method is considered preliminary and will be modified in the forthcoming version 8 data set.

For large aerosol extinction, e.g., in the polar regions and in the tropics where ice clouds are present, the version 7 processing relaxes to climatology in an unsatisfactory manner, resulting in low extinction values in regions of thick clouds. Version 8 data processing will handle these situations in a different manner, stating that the extinction is large, with the extinction set to a value of 0.02 km^{-1}, when thick clouds are encountered. For the version 7 (and 8) data the retrievals of the gaseous species are also impacted in regions of dense clouds, since the large cloud optical depths produce saturated emission.

Examples of synthetic spectra, for blockers 3, 4, and 9, near 6.23, 7.95, and 12.82 μm, respectively, are presented in Figures 1 and 2 to illustrate the impact of aerosol upon atmospheric emission. The calculations in Figures 1 and 2 are representative of 40°S latitude on April 22, 1992, at an altitude near 20 km. This is an altitude level for which the Pinatubo aerosol cloud is thick. The GENLN2 [*Edwards*, 1992] line-by-line radiative transfer model was used to calculate the emission spectra and radiance profiles. The mixing ratio profiles used in these calculations are CLAES 3AT zonal means for the latitude band between 37.5° and 42.5°S. Climatology was used for those species not retrieved by UARS.

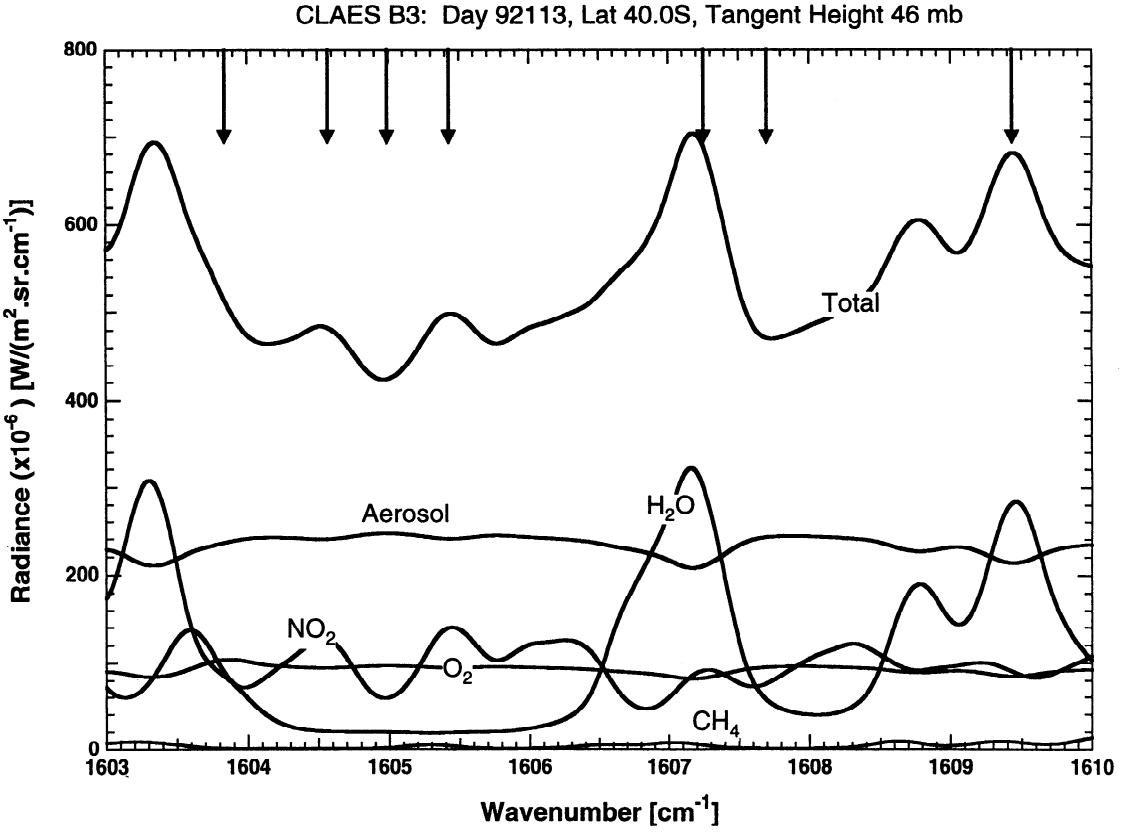

Figure 1a. Calculated emission spectra for Cryogenic Limb Array Etalon Spectrometer (CLAES) blocker 3, on April 22, 1992, at 40°S and 46 hPa. The arrows mark the CLAES observation channels. Total and component radiances are displayed.

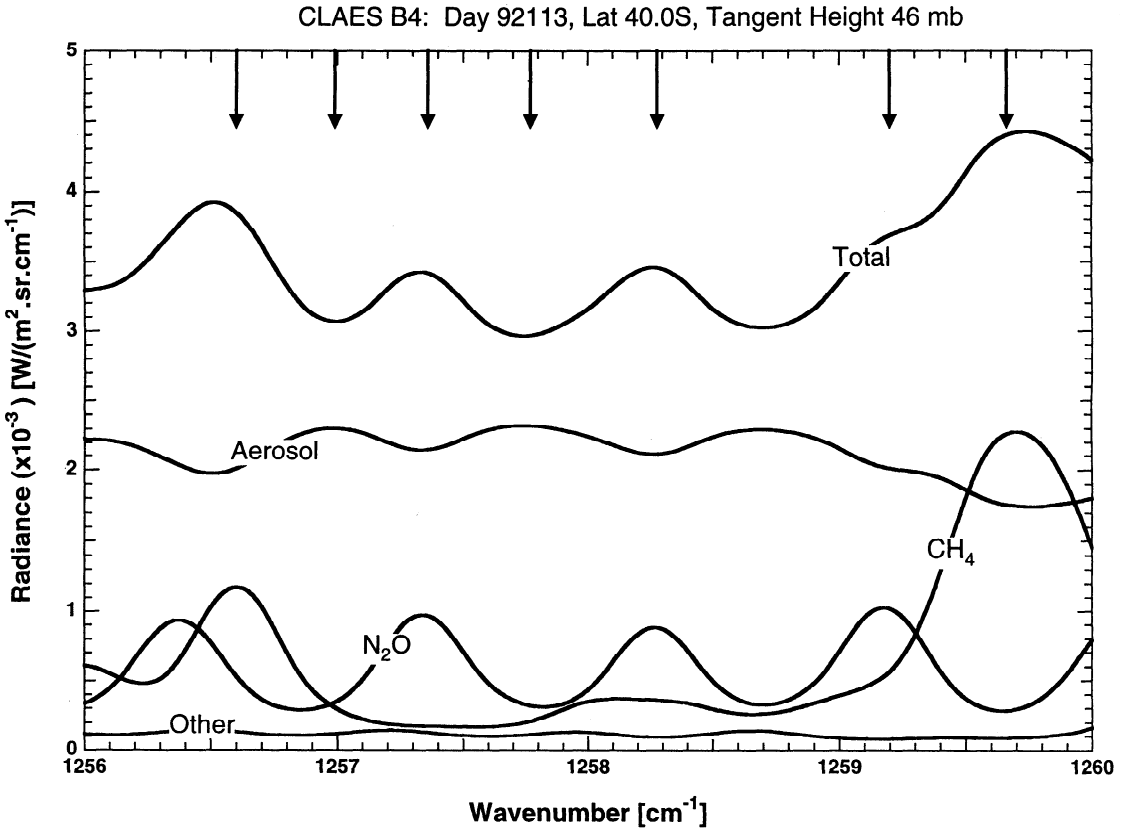

Figure 1b. Calculated emission spectra for CLAES blocker 4, on April 22, 1992, at 40°S and 46 hPa. The arrows mark the CLAES observation channels. Total and component radiances are displayed.

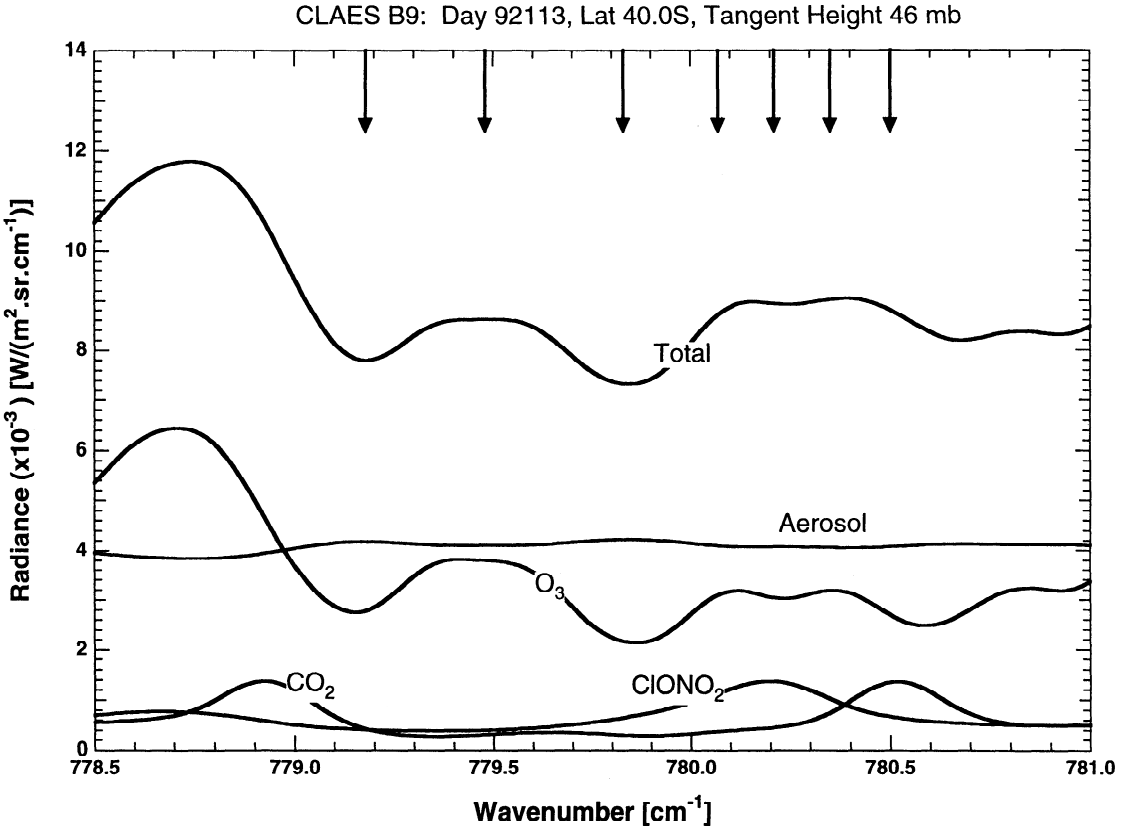

Figure 1c. Calculated emission spectra for CLAES blocker 9, on April 22, 1992, at 40°S and 46 hPa. The arrows mark the CLAES observation channels. Total and component radiances are displayed.

The aerosol extinction profiles are based upon CLAES data, though the falloff with altitude, in the vicinity of 10 hPa, is modeled using SAGE II aerosol extinction profiles.

The emission curves in Figures 1a–1c show the radiance contributions of each of the radiatively active species in the three spectral regions. The plots also show the positions of the CLAES channels, formed by stepping the etalon associated with each blocker region. All the radiatively active species are included in the calculation of each of the radiance components, which are calculated through all of the atmospheric layers and which sum to give the curve "total." For this reason the aerosol component reflects the spectral structure of the absorption lines of the other radiatively important gases. Profiles of the limb radiance for a series of limb view tangent heights, for one channel in each of the three blocker regions, are presented in Figures 2a–2c. These graphs show how the relative contributions from aerosol and the different emitting gases change with altitude. It is apparent from Figures 1 and 2 that the Pinatubo aerosol cloud introduced an important component to the radiance profiles observed by CLAES.

3. Sensitivity Study

Error analyses are presented in companion papers by *Roche et al.* [this issue], *Mergenthaler et al.* [this issue], *Kumer et al.* [this issue], and *Gille et al.* [this issue] for CLAES observations of N_2O and CH_4, $ClONO_2$, HNO_3, and temperature. Tables 4-7 display systematic and random error terms for the aerosol data, based upon similar calculations, for observations at 7.95 and 12.82 μm. The precision and accuracy terms are for data observed at midlatitude (35°N), on Janaury 10, 1992. The reader is referred to the companion papers for definitions of the terms used in Tables 4-7.

From Tables 4 and 5 the largest error terms are those due to uncertainties in the temperature retrieval. The systematic errors in Tables 4 and 5 are of the order of 10% for both the 7.95- and the 10.82-μm observations. From Tables 6 and 7, random error terms are of the order of 5%, with largest contributions again due to uncertainties in the temperature retrieval.

In sections 4 and 5 below, empirical precisions and accuracies will be assessed from CLAES data and correlative measurements. In section 6 a table of empirical accuracies is constructed, based upon the observational data and correlative measurements. The empirical accuracies will then be compared to the terms cited in Tables 4–7.

4. Precisions Derived From Retrieved Aerosol Extinction

Consecutive UARS orbits overlay each other at the northern and southern latitude extremes each day. This feature of orbital geometry allows precision values to be estimated for the retrievals of the CLAES aerosol extinction. Assuming that the aerosol extinction at a particular location does not vary substantially over the orbital period of 95 min, comparisons of aerosol extinction profiles, from consecutive UARS orbits, provide a reasonable upper limit to the variability of the extinction retrieval (see *Lambert et al.*, [this issue], for a discussion of this technique and for additional CLAES precision calculations). Precision values were estimated using data observed for consecutive orbits, for points separated in longitude and latitude by less than 1° and 2°, respectively. Figure 3 presents the calculated precision values for time periods between January 1992 and April 1993. Table 8 lists the time periods, the latitudes at which the calculations were made, and the number of coincident cases for each determination. The values in the figures are root mean square percent differences

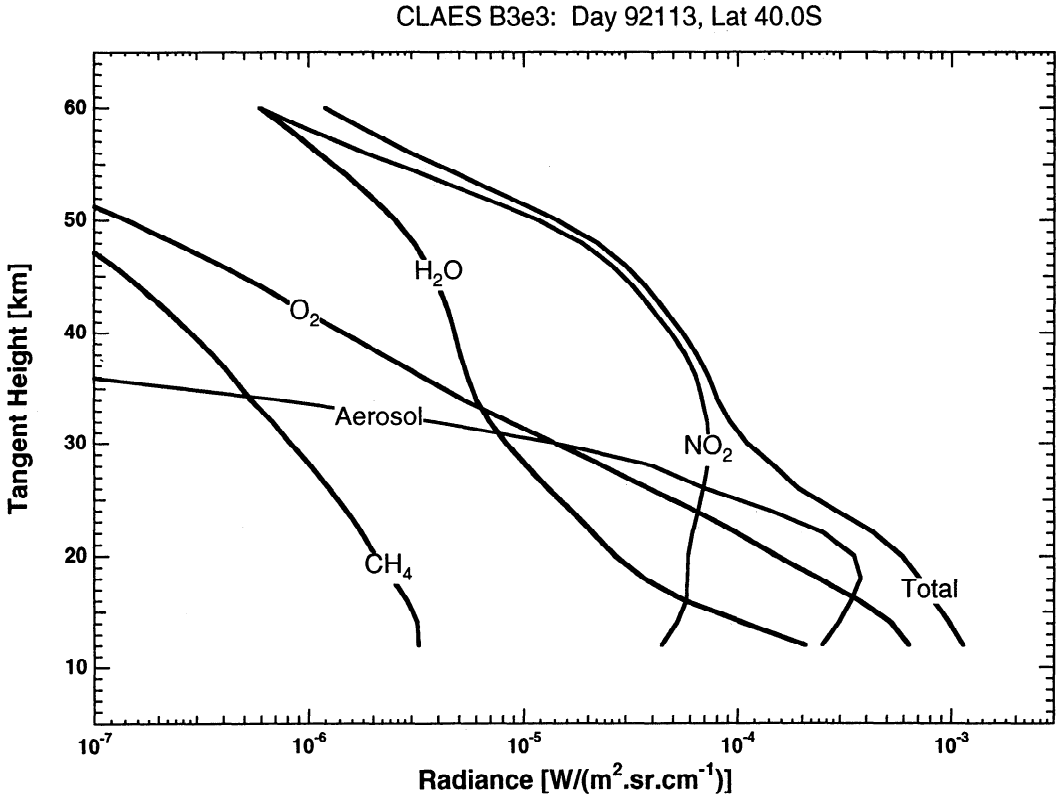

Figure 2a. Calculated radiance profiles for CLAES blocker 3, on April 22, 1992, at 40°S, for etalon position 3 (1604.99 cm^{-1}). Total and component radiance contributions are presented.

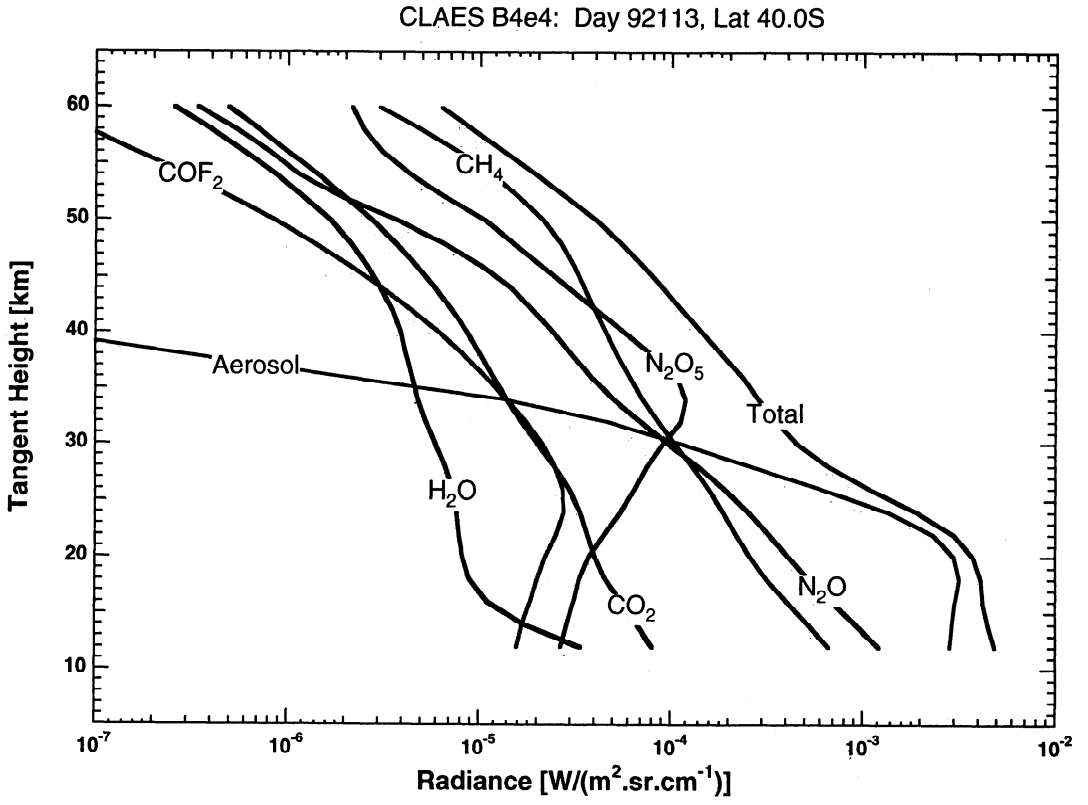

Figure 2b. Calculated radiance profiles for CLAES blocker 4, on April 22, 1992, at 40°S, for etalon position 4 (1257.77 cm^{-1}). Total and component radiance contributions are presented.

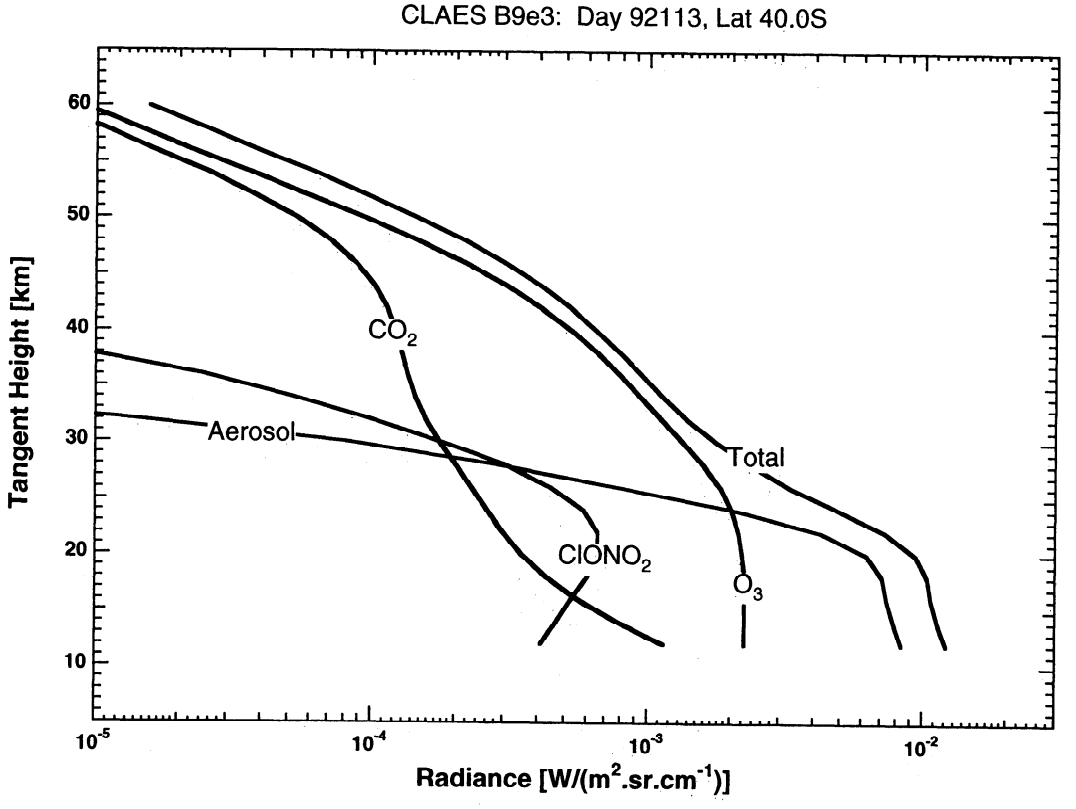

Figure 2c. Calculated radiance profiles for CLAES blocker 3, on April 22, 1992, at 40°S, for etalon position 3 (779.83 cm^{-1}). Total and component radiance contributions are presented.

Table 4. Systematic Errors (%) for Blocker 4 (7.95 μm, 1257 cm^{-1}) Aerosol Data

Term	Pressure, hPa 90	40	20	10
Radiometric cal	1.9	1.4	1.4	2.8
Spectral cal	1.0	0.8	0.6	0.6
Array dispersion	1.6	1.4	0.9	0.3
Detector spatial response	0.4	0.8	1.8	0.8
Optical cross talk	0.3	0.2	0.2	0.4
Retrieved temperature	12.1	9.5	8.0	7.6
Forward radiance	1.6	1.2	1.0	1.0
Root-sum-square (rss)	13.4	10.5	8.9	8.7

Table 6. Random Errors (%) for Blocker 4 (7.95 μm, 1257 cm^{-1}) Aerosol Data

Term	Pressure, hPa 90	40	20	10
Radiometric cal	0.9	0.7	0.6	0.6
Spectral cal	1.6	1.2	1.0	1.0
Horizontal gradients	1.6	1.2	1.0	1.0
Vertical smear	0.5	1.1	2.4	1.1
Retrieved temperature	3.7	3.0	2.7	2.6
Noise	0.1	0.1	0.4	0.9
Rss	4.4	3.7	3.9	3.3

at the standard UARS pressure levels of 10, 14, 21, 31, 46, 68, and 100 hPa. All extinction values were used in the calculations; that is, no high or low values were excluded.

The precision values for August 8–11, 1992, are larger than those for the other time periods, for reasons which are not clear. Precisions for blocker 4 (7.95 μm, 1257 cm^{-1}) become large for pressures less than 20 hPa. This is due to the ambiguity in differentiating between the aerosol and the N_2O_5 component of the emission signal. Some of the precision curves show an altitude dependence, with larger percent values at pressure levels less than 20 hPa and at 100 hPa. This is expected since the aerosol extinction profiles for CLAES, other UARS, and other satellite instruments generally decrease in magnitude between 20 and 30 km altitude. At the largest pressure levels the retrievals frequently become more difficult as the limb-viewing ray paths become optically thick from both gaseous and aerosol species.

Table 9 presents average precision values based upon the data displayed in Figure 3. To obtain the average precisions, an average of the data in Figure 3 was calculated, excluding the data points for the August 8–11, 1992, time period. On average, most of the precision values are between 10 and 25%.

5. Comparison With Correlative Measurements

Aerosol correlative measurements are next compared to the CLAES extinction values. Sources of correlative measurements include particle size distributions, SAGE II extinction data, ATMOS transmission spectra, and other UARS experiments. For the first three sources the comparisons are indirect, in that the correlative measurements need to be transformed or scaled before the correlative measurements can be compared to the CLAES data. The goal of all of the comparisons is to gain insight on the accuracy of the CLAES extinction data.

5.1. Comparison With Balloonsonde Measurements

In situ particle size distributions have been measured over Laramie, Wyoming (41°N latitude and 254°E longitude) for dates before and after the June 12–16, 1991, eruptions of Mount Pinatubo [*Deshler et al.*,1993]. These measurements covered the altitude range between 10 and 32 km. The particle size distributions, represented by bimodal (or monomodal) lognormal fits to the observations, were measured at every 1 km of altitude. During the January 1992 through April 1993 time frame, there were seven coincident particle size distribution profiles which can be used for validation purposes. Table 10 lists the seven dates of the observations, the distances between the CLAES and in situ observations, and the CLAES 1605 cm^{-1} extinctions at 46 hPa. The extinctions from the earlier dates contribute more to the mean profile than the later dates, since the aerosol extinction decreases with time.

To use the particle size measurements, Mie calculations were performed to predict the infrared extinction coefficients, which were then compared to the measured CLAES extinction. The CLAES and Wyoming measurements were separated in distance by between 101 and 409 km, with an average spacing of 258 km. Input to the theoretical Mie calculations, at each altitude level of the in situ data, included the measured particle size distributions, temperatures, and water vapor mixing ratios. The water vapor mixing ratios are those observed by the MLS on UARS. The water vapor data are used to estimate the H_2SO_4 acidity (by weight), using the thermodynamic equilibrium calculations of *Steele and Hamil* [1981]. The complex indices of refraction of sulfate aerosol, assumed to consist of H_2SO_4 droplets, are dependent upon the H_2SO_4 acidity. In this study we use the room temperature indices of *Palmer and Williams* [1975], and those of *Remsberg et al.* [1974] in independent calculations. The temperature dependence of the indices are estimated by invoking the Lorentz-Lorentz relationship. When the theoretical extinction profile was calculated, extinction values were interpolated to the standard UARS pressure levels.

The reason the *Palmer and Williams* [1975] and *Remsberg et al.* [1974] indices are used in independent calculations is that the tabulations have appreciably different imaginary indices between 8 and 12 μm. Table 11 lists the real and imaginary indices from the two tabulations, for the case of 75% H_2SO_4, at room temperature. The Remsberg tabulation ranges between 747 and 1571 cm^{-1}, while the Palmer and Williams tabulation covers the

Table 5. Systematic Errors (%) for Blocker 9 (12.82 μm, 780 cm^{-1}) Aerosol Data

Term	Pressure, hPa 90	40	20	10
Radiometric cal	1.3	1.3	1.3	2.4
Spectral cal	0.7	0.7	0.6	0.6
Spectral response	3.3	3.3	3.0	3.0
Array dispersion	1.1	1.3	0.9	0.3
Detector spatial response	1.5	1.1	1.4	1.8
Optical cross talk	0.2	0.2	0.2	0.2
Retrieved temperature	5.7	6.4	5.3	5.4
Forward radiance	1.1	1.1	1.0	1.0
Rss	7.0	7.6	6.6	6.4

Table 7. Random Errors (%) for Blocker 9 (12.83 μm, 780 cm^{-1}) Aerosol Data

Term	Pressure, hPa 90	40	20	10
Radiometric cal	0.6	0.6	0.6	0.6
Spectral cal	1.1	1.1	1.0	1.0
Horizontal gradients	1.1	1.1	1.0	1.0
Vertical smear	0.5	1.6	5.7	1.8
Retrieved temperature	2.1	1.9	1.7	1.6
Noise	0.1	0.1	0.6	1.7
Rss	2.7	3.0	6.2	3.3

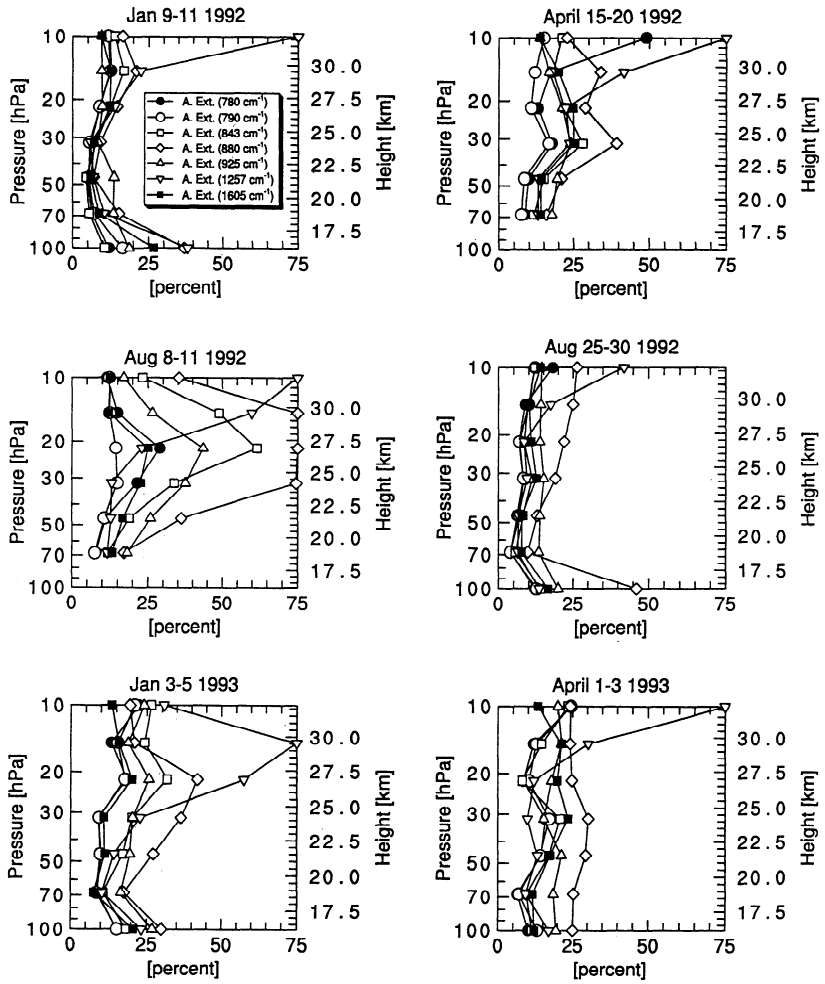

Figure 3. CLAES precisions for January 9–11, 1992, April 15–20, 1992, August 8–11, 1992, August 25–30, 1992, January 3–5, 1993, and April 1–3,1993.

400 to 27800 cm^{-1} range. Representative aerosol extinction spectra were calculated using the two tabulations, and Table 11 cites the ratio of extinction "Remsberg/PW" to indicate the sensitivity of extinction to the complex index of refraction. The ratios in Table 11 imply that the comparisons between the theoretical extinction and that of the CLAES experiment, discussed in the following paragraphs, are limited by the uncertainties in the indices. As cold temperature indices become available, the comparison uncertainties will diminish.

Figure 4 presents the average extinction profile at 6.23 μm (1605 cm^{-1}) for the CLAES data and the average extinction profile based upon the size distribution data. The shapes of the two curves are similar, but the CLAES profile values are larger than the theoretical values. It is apparent that the CLAES data at 6.23 μm has values larger than the theoretical mean for all pressure levels.

Table 8. Dates, Latitudes, and Number of Comparisons for Precision Estimates

Days	Year	Latitude	Number of Comparisons
January 9–11	1992	32°S	42
April 15–20	1992	32°N	83
August 8–11	1992	32°S	37
August 25–30	1992	32°N	82
January 3–5	1993	32°S	39
April 1–3	1993	32°N	39

Figures 5a and 5b display the ratios of CLAES and theory values using the two refractive index tabulations. It is apparent that the ratios based upon the Remsberg indices form a set which are closer to the ideal comparison of unity. Both calculations and all blocker regions, however, have ratios appreciably greater than unity for pressures less than 46 hPa. The ratios are closest to unity at 46 and 68 hPa.

The overestimation of the CLAES extinction in Figures 5a and 5b, at pressure levels less than 46 hPa, is also seen in ISAMS and HALOE data. Figure 3 of *Hervig et al.* [1993] shows HALOE extinction data generally larger than the theoretical extinction over Laramie, Wyoming, for August 8, 1992, at pressures less than 50 hPa. In the work of *Lambert et al.* [this issue], ISAMS and theoretical extinction profiles are compared over Laramie, for six dates in 1991 and 1992. The ISAMS extinctions are factors of 9.7 and 4.8 times larger than the Mie theoretical values near 20 and 30 hPa, at 6.2 μm, and factors of 7.3 and 3.4 times larger at 12.1 μm. These factors are similar to those displayed for the CLAES data in Figure 5b. It is possible that the theoretical calculations are misleading at the smallest pressure levels or that excess instrumental radiance (for the emission experiments) and the radiative contributions from minor gases (for the emission and

Table 9. Average Precision Values (%) Based on Figure 3

Wavelength, μm	Wavenumber, cm^{-1}	Pressure, hPa						
		10	14	21	32	46	68	100
12.82	780	25	13	11	11	9	7	12
12.65	790	17	13	11	11	9	7	14
11.90	840	19	17	17	17	12	9	14
11.36	880	22	25	27	27	20	17	35
10.83	925	16	16	18	17	18	16	21
7.95	1257	72	42	23	14	11	10	23
6.23	1605	13	16	18	16	11	10	19

occultation experiments) are being misinterpreted as an aerosol component.

5.2. Comparison With SAGE Extinction Data

SAGE II has measured extinction profiles from the Earth Radiation Budget Satellite (ERBS) since October 1984. The SAGE II occultation extinction measurements are made at 1.02, 0.525, 0.453, and 0.385 μm, with accuracies of the order of 10, 20, 20, and 20%, respectively [*Russell and McCormick*, 1989]. The measurements are global in coverage between 80°N to 80°S. In this study we compare scaled SAGE II extinction profiles at 0.525 μm to CLAES extinction profiles.

Table 12 lists the scaling factors which are used to transform the SAGE extinction at 0.525 μm to each of the CLAES wavelengths. Two sets of scaling factors are presented, based upon the two tabulations of refractive indices discussed in section 5.1. The scaling factors are based upon Mie calculations, using the Wyoming particle size distributions for the June–September 1992 time period. Since particle size distributions evolve with time, the scaling factors in Table 12 are approximate. The scaling factors, of the order of 2.0×10^{-2} to 1.8×10^{-1}, are averages for the June–September 1992 time period. Individual scaling factors vary by roughly 40% from the averages listed in Table 12.

Forty-three SAGE extinction profiles were averaged between August 25, 1992, and August 30, 1992, for latitudes between 44°S and 55°S. The average SAGE profile at 0.525 μm was then scaled by the factors in Table 12, and the scaled SAGE profiles were then compared to the averaged CLAES extinction data (averaged over the 43 SAGE observation positions). The CLAES extinction data used in this comparison are extracted from our mapped version of the CLAES profile data. The SAGE and CLAES data differed on average by 2° in latitude and 3° in longitude. Figure 6 compares the SAGE and CLAES average extinction profiles at 6.23 μm (1605 cm^{-1}). As with Figure 4, the largest differences in the two profiles occur at the low- and high-pressure limits of the graph.

Figures 7a and 7b display the ratios of CLAES and SAGE extinction. It is apparent that the ratios based upon the Remsberg indices form a set of ratio curves which are closer to the ideal comparison of unity. Both figures, however, have ratios appreciably greater than unity for pressures less than 46 hPa.

There is a consistent pattern displayed by the ratios presented in Figures 5 and 7. At pressure levels of 46 and 68 hPa, the ratios at 780 and 790 cm^{-1} are larger than unity, while the ratios at 925 and 880 cm^{-1} are near or below unity.

5.3. Comparison With ATMOS Data

Rinsland et al. [1994] derived a sulfate aerosol transmission spectrum from ATMOS observations on April 1, 1992, at 54°S latitude and 39°E longitude at 20.9 km altitude. The CLAES experiment also observed the southern hemisphere at this time. While the comparisons in sections 5.1 and 5.2 are dependent upon uncertain refractive indices, a direct transmission observation is independent of theoretical uncertainties. However, as discussed by Rinsland, there are observational uncertainties in the unity transmission level of the ATMOS data. Rinsland renormalized the ATMOS transmission spectrum, by factors between 0.88 and 0.93, in comparisons with theoretical transmission (based upon application of SAGE II retrievals of the aerosol size distribution in a Mie calculation). The need to renormalize the ATMOS data is likely due to both instrumental uncertainties and uncertainties in the Mie calculations.

Figure 8 compares scaled ATMOS extinction and averaged CLAES extinction on April 1, 1992, for the latitude range 52° to 56°S and the longitude range from 35° to 45°E. The comparison is based upon the transmission spectrum displayed in panel C of Rinsland's Figure 3. Six CLAES and six ISAMS spectral data points are included in the comparison. The CLAES spectrum was calculated by first normalizing the average CLAES spectrum to unity at 1605 cm^{-1}. This normalization factor was also used to normalize the ISAMS data points. This procedure yielded a set of nine extinctions, y_{UARS}, with the 1897 cm^{-1} CLAES extinction excluded from the set. The ATMOS data points were obtained by calculating the optical depths of the ATMOS transmission, which were then normalized to unity at 1605 cm^{-1}. This yielded a set y_{ATMOS} at the corresponding y_{UARS} wavenumber positions. The

Table 10. Dates, 46 hPa Extinction, for the CLAES/Wyoming Comparisons

Day	Year	Extinction 1.0×10^{-4} km^{-1}	Distance, km
March 6	1992	10.2	409
May 8	1992	5.58	268
May 29	1992	4.42	293
July 17	1992	3.71	270
August 8	1992	2.78	101
October 23	1992	1.95	370
February 26	1993	2.21	355

The extinctions are CLAES 1605 cm^{-1} values, corrected for pressure-induced absorption. The distances are those between the CLAES and the Laramie observations.

Table 11. Sensitivity of Extinction Spectra to Imaginary Refractive Indices

Wavelength, μm	Wavenumber, cm^{-1}	RM_{im}	PW_{im}	Ratio
12.82	780	0.25	0.19	1.7
12.65	790	0.24	0.19	1.6
11.90	840	0.32	0.21	1.7
11.36	880	0.48	0.36	1.3
10.83	925	0.44	0.26	1.4
7.95	1257	0.52	0.42	1.1

"Ratio" refers to the ratio of extinction (Remsberg/Palmer and Williams). PW_{im} are representative imaginary indices of *Palmer and Williams* [1975]. RM_{im} are representative imaginary indices of *Remsberg et al.* [1974].

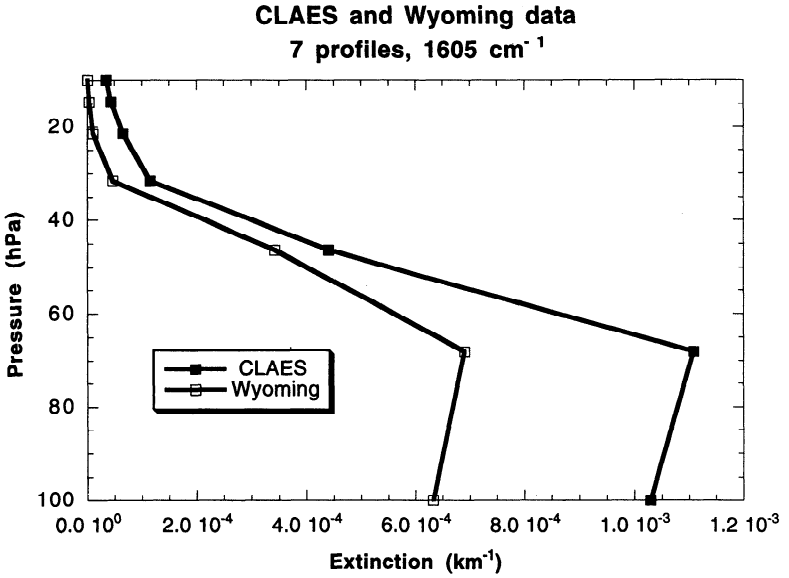

Figure 4. CLAES and Wyoming average extinction profiles at 1605 cm^{-1} (6.23 μm). The Wyoming values are Mie theoretical predictions which used observed particle size distributions.

ATMOS spectrum was then multiplied by a factor f, which minimized the differences (y_{UARS} - f*y_{ATMOS}).

The comparison in Figure 8 shows that the three experiments are reporting similar spectral features characteristic of sulfate aerosol. For this range of wavenumber the extinction peak is in the vicinity of 1200 cm^{-1}, while the observations at the other wavelengths show lesser extinction. The CLAES 780 and 790 cm^{-1} data points are higher than the ATMOS data, while the 925 cm^{-1} data point is below the ATMOS value. These qualitative offsets are consistent with the results presented in sections 5.1 and 5.2, since the ratios at 780 and 790 cm^{-1} are greater than unity, while the 925 cm^{-1} ratios are less than unity near 20 km, in Figures 5 and 7.

5.4. Aerosol Retrieval Bias

The 12.82-μm (790 cm^{-1}) extinctions are larger than those at 12.65 μm (780 cm^{-1}) in Figures 4-8. This is contrary to theoretical expectation. Theoretical calculations for 1992, based upon the Wyoming size distributions, yield ratios of extinction (780 cm^{-1} to 790 cm^{-1}) near 0.97. Figure 9 presents ratios of zonal average extinction at the two wavelengths at 20°S and 20°N latitude. It is apparent that the ratios represent a difference in extinction of 30% at the two wavelengths.

The ratios become larger toward the end of the CLAES operational period. A graph of extinction versus extinction ratio shows that the ratios become larger as extinction decreases. This correlation is likely responsible for the rise in ratio values past UARS day 400 (October 15, 1992), since the Mount Pinatubo aerosol cloud decreases its extinction signal with time.

A partial explanation for why the 12.65-μm extinctions are larger than the 12.82-μm extinctions is that there are radiative contributions to the total radiance which are not accounted for in the operational CLAES retrieval. $ClONO_2$, NO_2, HNO_3, and CCl_4 all contribute to the total radiance near 12.65 μm. At 25 km,

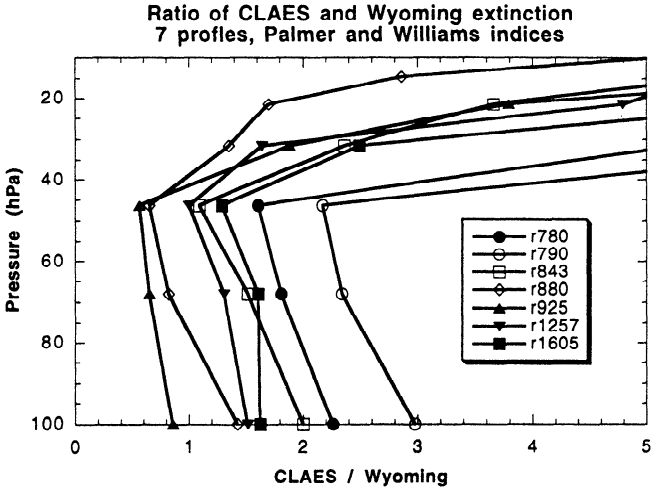

Figure 5a. Ratios of CLAES and Wyoming average extinction profiles for seven CLAES filter regions, using the *Palmer and Williams* [1975] refractive indices.

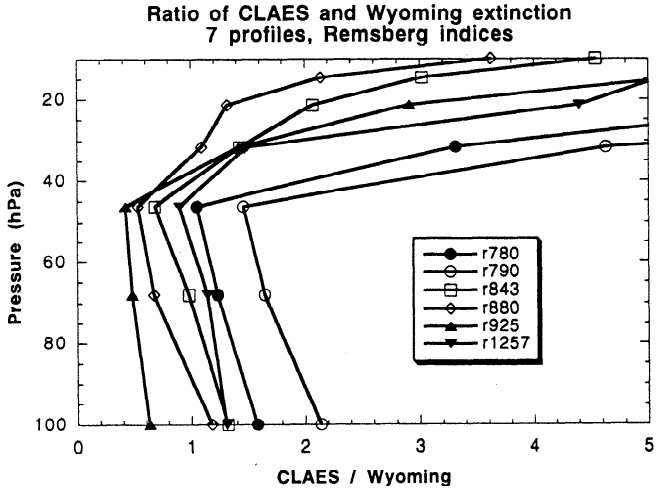

Figure 5b. Ratios of CLAES and Wyoming average extinction profiles for six CLAES filter regions, using the *Remsberg et al.* [1974] refractive indices.

Table 12. Theoretical Scaling Factors CLAES/(SAGE 0.525 μm)

Wavelength, μm	Wavenumber, cm^{-1}	Theoretical Scaling Factor PW	RM
12.82	780	$2.05x10^{-2}$	$3.50x10^{-2}$
12.65	790	$2.05x10^{-2}$	$3.41x10^{-2}$
11.90	840	$2.49x10^{-2}$	$4.39x10^{-2}$
11.36	880	$4.87x10^{-2}$	$6.37x10^{-2}$
10.83	925	$6.00x10^{-2}$	$7.67x10^{-2}$
7.95	1257	$1.63x10^{-1}$	$1.75x10^{-1}$
6.23	1605	$5.01x10^{-2}$	
5.27	1897	$6.55x10^{-2}$	

Values are based upon Mie calculations which used Wyoming size distributions. PW, based upon *Palmer and Williams* [1975] refractive indices. RM, based upon *Remsberg et al.* [1974] refractive indices.

for example, these gases have a radiance contribution near 5% of the aerosol radiance contribution. These radiative contributions, however, account for only 15% of the 30% difference cited above.

Averages of the ratios in Figure 9 and averages of ratios at the other pressure levels are presented in Table 13. The bias estimates in Table 13 are used in section 6 to construct a table of empirical accuracies, with precisions supplied by the orbit-to-orbit values of Table 9. While the bias values in Table 9 apply only to a systematic offset in the 12.65- and 12.82-μm data, they are useful as estimates of bias for the other blocker regions.

ISAMS and CLAES extinction can also be used to estimate the CLAES bias at 6.23 μm. Calculated RMS differences of zonally averaged CLAES and ISAMS extinction, for days in early April 1992, are presented in Table 13 (in the "RMS offset" column). Section 6 will use these RMS offsets if they are larger than the 12.65 μm/12.82 μm biases. At 100 hPa the offset is near 100%, due to the fact that the CLAES 6.23-μm data need to be corrected for pressure-induced absorption of oxygen (see Table 2). One must be particularly careful with the 6.23-μm extinction at 100 hPa, since the process of PIA correction can produce a corrected extinction which is less than zero.

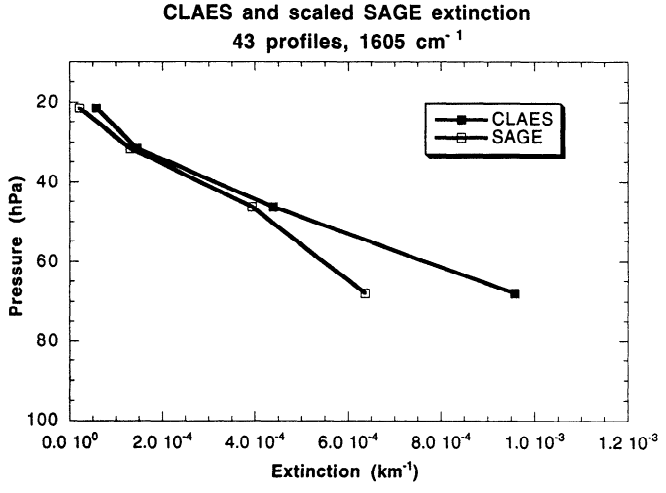

Figure 6. CLAES and scaled Stratospheric Aerosol and Gas Experiment (SAGE II) average extinction profiles at 1605 cm^{-1} (6.23 μm), for 43 SAGE profiles. The scaling factors are from Mie theoretical predictions, which used observed particle size distributions.

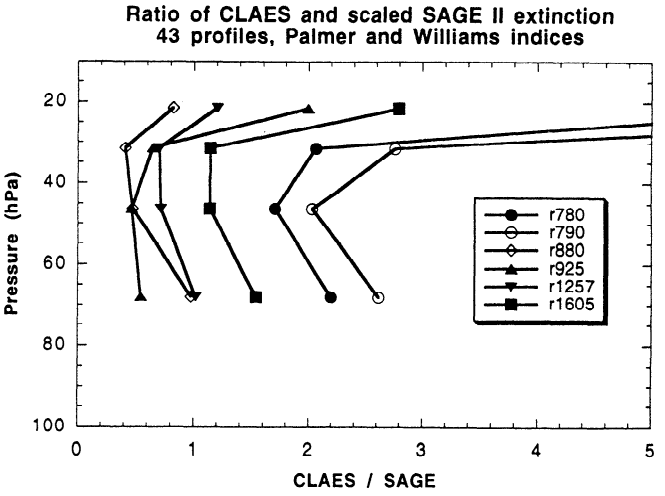

Figure 7a. Ratios of CLAES and scaled SAGE II average extinction profiles for six CLAES blocker filter regions, using the *Palmer and Williams* [1975] refractive indices.

5.5. Spectral Comparison With ISAMS and HALOE Data

Additional comparisons of UARS extinction data and sulfate extinction spectra are contained in Figures 10 and 11. Figure 10 presents a comparison of the sulfate theoretical spectrum with CLAES and ISAMS data. The graph was constructed in the following manner: The observations are a result of coadding 1095 CLAES spectra and 1095 ISAMS spectra, observed between April 20 and April 22, 1992, at 46 hPa, for latitudes between 16°N and 32°N. After coadding, the observations were normalized to unity at 790 cm^{-1}. The theoretical sulfate spectra, based upon application of the *Palmer and Williams* [1975] refractive indices, was normalized by finding, by least squares analysis, the scaling factor which produced the lowest RMS fit of the normalized CLAES data to the theoretical curve (that is, all of the theory curve points were multiplied by the same least squares scaling factor). For the range of latitude and time of year used to coadd the observations, the stratospheric temperatures and locations support the existence of sulfate aerosol. It is apparent that both

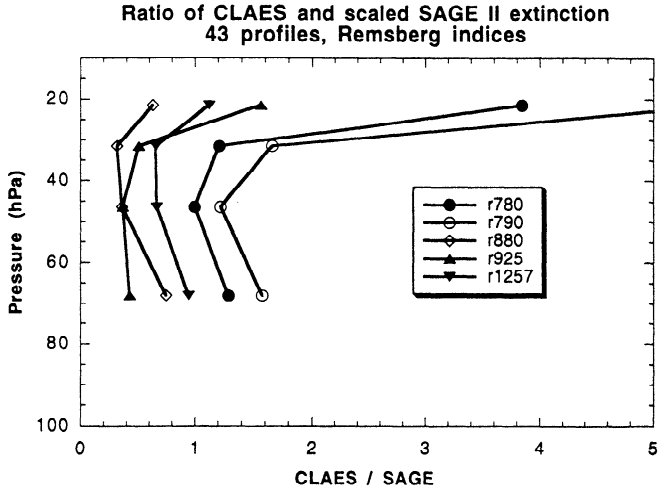

Figure 7b. Ratios of CLAES and scaled SAGE II average extinction profiles for five CLAES filter regions, using the *Remsberg et al.* [1974] refractive indices.

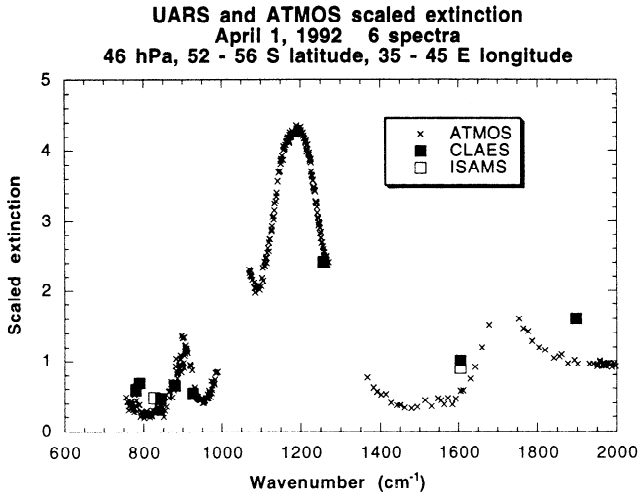

Figure 8. Comparison of normalized CLAES and ISAMS extinctions with a scaled ATMOS sulfate spectrum, observed on April 1, 1992, at 52°S latitude, at 20.9 km altitude [*Rinsland et al.*, 1994].

the CLAES and the ISAMS data conform to the general shape of the sulfate theory curve. Similar graphs (not shown) at 68 and 31 hPa also show the conformity. The CLAES data point at 1897 cm^{-1} is substantially above the theory curve. This is likely due to the fact that a daytime component in the emission is present, i.e. the daytime extinction is larger than the nighttime extinction. The enhanced emission is being interpreted by the production software as a large value of aerosol extinction.

Figure 11 displays a comparison of the sulfate theoretical spectrum with CLAES and HALOE data. The observations are a result of coadding 22 HALOE spectra and coadding 22 CLAES spectra for the HALOE positions and times. The CLAES and HALOE data were observed between August 22 and August 24, 1992, at 68 hPa for latitudes between 30°S and 41°S. The normalization procedure is that used for Figure 10. For the range of latitude and time of year used to coadd the observations, the stratospheric temperatures and locations support the existence of

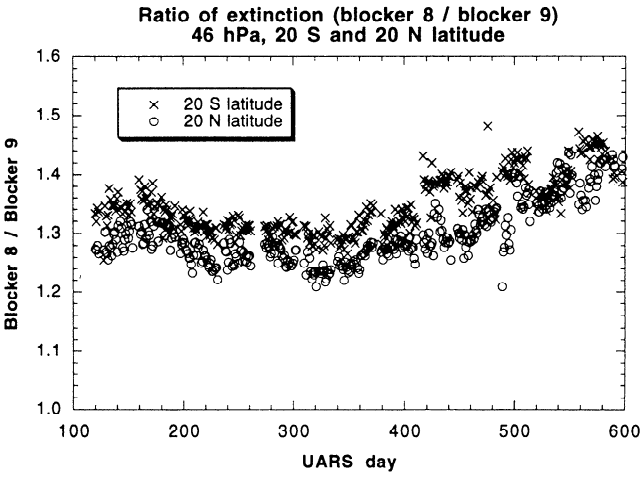

Figure 9. Ratios of blocker 8 (12.65 μm) and blocker 9 (12.82 μm) zonal averages of extinction at 46 hPa, at 20°S and 20°N latitude. UARS days 100 and 600 correspond to December 20, 1991, and May 3, 1993.

Table 13. Estimated Percent Biases and Offsets

Pressure	Bias	RMS Offset
21	34	53
31	31	19
46	32	21
68	33	26
100	25	115

"Bias" refers to differences between 12.65- and 12.82-μm zonal averages. "Offset" refers to RMS differences of ISAMS and CLAES 6.23-μm zonal averages, after the CLAES data have been corrected for PIA.

sulfate aerosol. In accord with the comparison presented in Figure 10, the CLAES and HALOE data of Figure 11 conform to the general shape of the sulfate theory curve. At 100 hPa there is also conformity, while at 31 hPa, the HALOE data fall below the theory curve, when the theory curve is scaled to the CLAES data. If the HALOE data are used to scale the theory curve, the CLAES data then lie above the theory curve. The discrepancy at 31 hPa (not shown) is likely due to the fact that CLAES likely overestimates extinction values at 31 hPa.

5.6. Comparison With ISAMS Data

The comparisons discussed above are limited in geographical coverage. Comparisons of CLAES data with ISAMS data allow analysis to extend globally, since the ISAMS instrument on UARS observes at the same times and places as CLAES. (This is true most of the time, though ISAMS can also view toward the sunward facing side of UARS, whereas CLAES only views the direction facing away from the Sun.) We mapped the level 3AT CLAES and ISAMS data, using both day and nighttime values, with the mapping granularity set at 5° in longitude and 4° in latitude. As discussed by *Lambert et al.* [this issue], the ISAMS systematic errors at 12.11 μm are estimated to be 4, 10, 18, and 34%

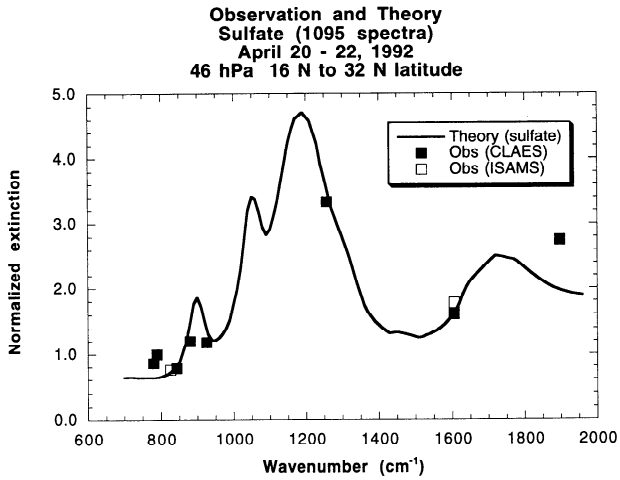

Figure 10. Comparison of observation and theory for sulfate aerosol. The observations are obtained by coadding 1095 mapped CLAES and Improved Stratospheric and Mesospheric Sounder (ISAMS) extinction observations for April 20–22, 1992, at 46 hPa, for latitudes between 16°N and 32°N. The theory curve is normalized by least squares fit at seven of the CLAES wavenumbers. The CLAES 1897 cm^{-1} point and the ISAMS data are excluded from the least squares fit, which solved for the scaling factor which was applied to the theoretical curve.

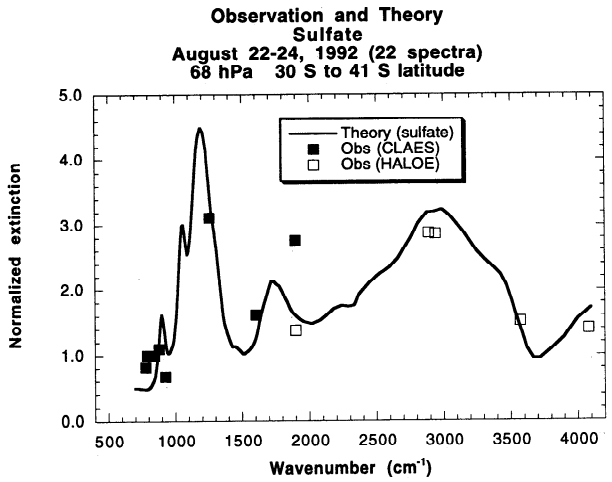

Figure 11. Comparison of observation and theory for sulfate aerosol. The observations are obtained by coadding 22 extinction observations for August 22–24, 1992, at 68 hPa, for lattidues between 30°S and 41°S. The theory curve is normalized by least squares fit to seven of the CLAES wavenumbers. The CLAES 1897 cm^{-1} point and the HALOE data are excluded from the least squares fit, which solved for the scaling factor which was applied to the theoretical curve.

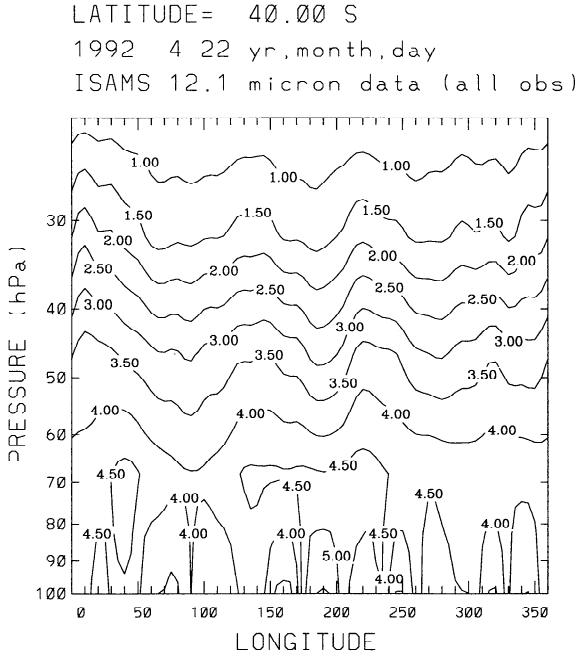

Figure 12b. ISAMS 12.11-μm (826 cm^{-1}) mapped extinction data for April 22, 1992, at 40°S. The extinction is in units of $1.0x10^{-4}$ km^{-1}.

at 68, 46, 32, and 22 hPa, respectively, and the random errors are estimated to be 29, 46, 44, and 58% at the four pressure levels.

Figure 12a displays CLAES 12.82-μm (790 cm^{-1}) mapped data for April 22, 1992, at 40°S, Figure 12b displays the 12.11-μm ISAMS data, and Figure 12c presents the percent differences, 100x(CLAES-ISAMS)/CLAES, for Figures 12a and 12b. The aerosol extinction in Figures 12a and 12b are in units of $1.0x10^{-4}$ km^{-1}. It is apparent that the longitudinal structure of the aerosol is similar for both instruments for pressure levels between 20 and 50 hPa. The ISAMS local maxima at 140° and 310°E longitude are suppressed in the CLAES data.

Figure 12c shows that the CLAES aerosol extinction is between 10 and 25% larger than the ISAMS extinction for most of the pressure range. The composition of the aerosol at 40°S is expected to be that of sulfate particles. Theoretical calculations for 1992, based upon the Wyoming size distributions, yield extinction ratios between 0.91 and 0.95 (12.82-μm extinction/12.11-μm extinction). Thus the CLAES extinction at 12.82 μm is 15 to 35%

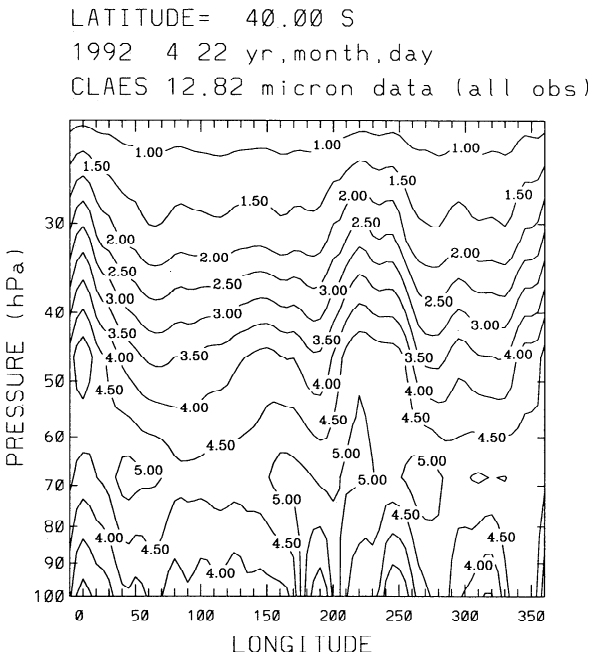

Figure 12a. CLAES 12.82-μm (780 cm^{-1}) mapped extinction data for April 22, 1992, at 40°S. The extinction is in units of $1.0x10^{-4}$ km^{-1}.

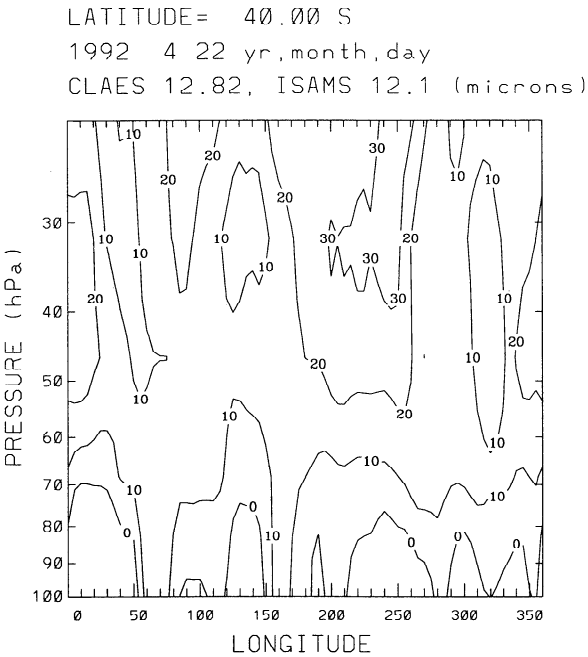

Figure 12c. Percent differences, 100x(CLAES-ISAMS)/CLAES, for the extinction data presented in Figures 12a and 12b.

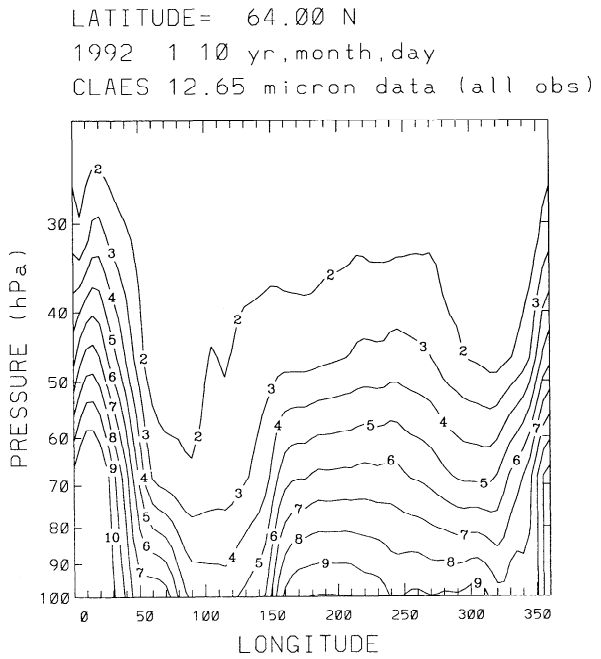

Figure 13a. CLAES 12.65-μm (790 cm^{-1}) mapped extinction data for January 10, 1992, at 64°N. The extinction is in units of 1.0×10^{-4} km^{-1}. A polar stratospheric cloud (PSC) is seen centered at 20° longitude.

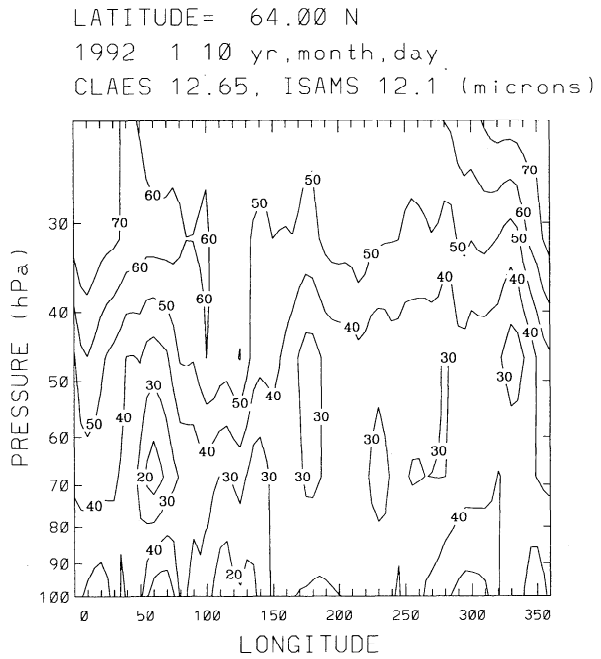

Figure 13c. Percent differences, 100x(CLAES-ISAMS)/CLAES, for the extinction data presented in Figures 13a and 13b.

larger than the ISAMS extinction, when the theoretical ratio of extinction is factored into the comparisons.

Figure 13a displays CLAES 12.65-μm (780 cm^{-1}) mapped data for January 10, 1992, at 64°N; Figure 13b displays the 12.11-μm ISAMS data; and Figure 13c presents the percent differences, 100x(CLAES-ISAMS)/CLAES, for Figures 13a and 13b. The aerosol extinction in Figures 13a and 13b are in units of 1.0×10^{-4} km^{-1}. It is apparent that the longitudinal structure of the aerosol is similar for both instruments for pressure levels between 20 and 100 hPa. The CLAES extinction is substantially higher than the ISAMS extinction between 0° and 50°E longitude. The extinction in this region is that of a polar stratospheric cloud (PSC) feature [*Taylor et al.*, 1994].

Figure 13c shows that the CLAES aerosol extinction is between 20 and 60% larger than the ISAMS extinction for most of the pressure range. The composition of the aerosol in Figure 13 is a combination of sulfate aerosol and that of PSCs. Theoretical calculations for 1992, based upon the Wyoming size distributions, yield extinction ratios for sulfate aerosol between 0.92 and 0.95 (12.65-μm extinction/12.11-μm extinction). Thus the CLAES extinction at 12.65 μm is 25 to 70% larger than the ISAMS extinc-

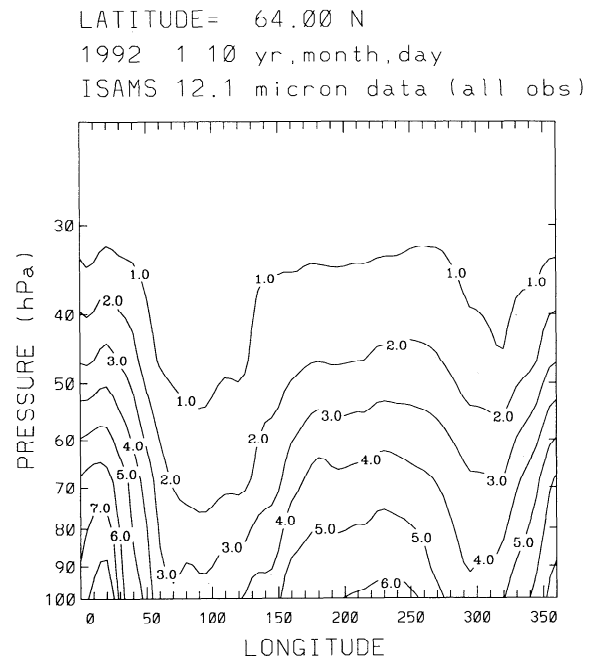

Figure 13b. ISAMS 12.11-μm (826 cm^{-1}) mapped extinction data for January 10, 1992, at 64°N. The extinction is in units of 1.0×10^{-4} km^{-1}. A PSC is seen centered at 20° longitude.

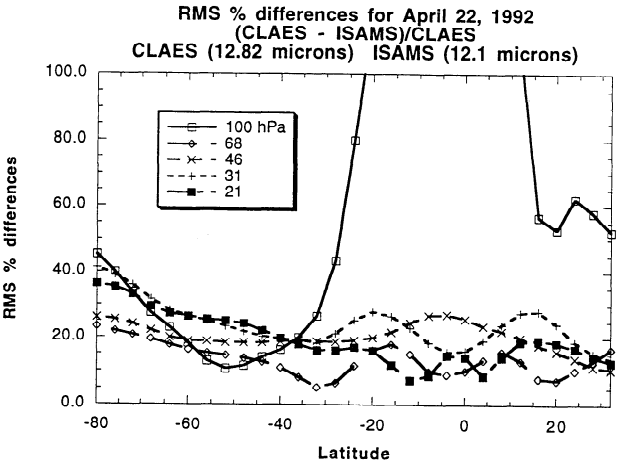

Figure 14a. RMS percent differences, 100x(CLAES-ISAMS)/CLAES, for April 22, 1992, for CLAES 12.82-μm and ISAMS 12.11-μm data, for 32°N to 80°S latitude, for 100, 68, 46, 31, and 21 hPa.

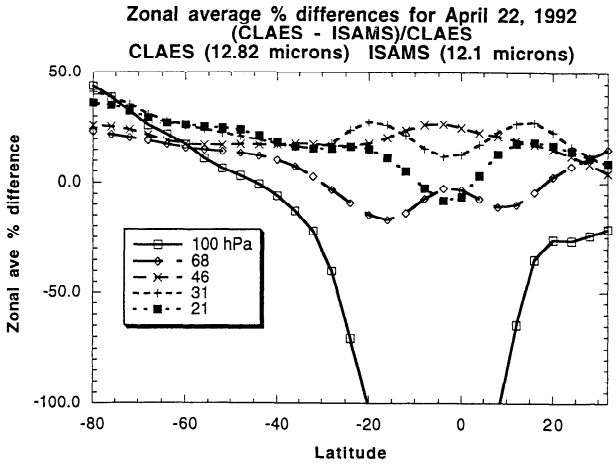

Figure 14b. Average percent differences, 100x(CLAES-ISAMS)/CLAES, for April 22, 1992, for CLAES 12.82-μm and ISAMS 12.11-μm data, for 32°N to 80°S latitude, for 100, 68, 46, 31, and 21 hPa.

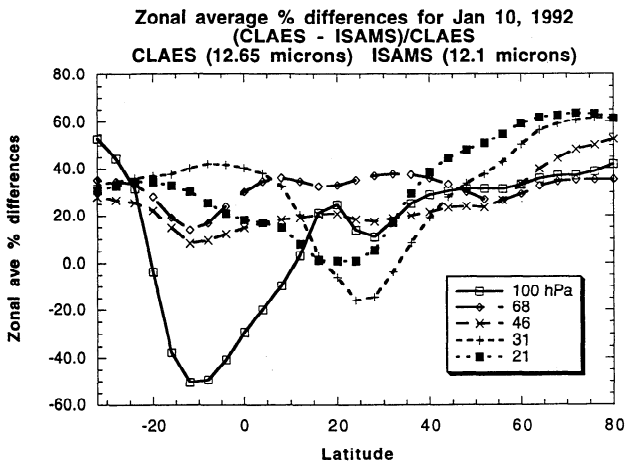

Figure 15b. Average percent differences, 100x(CLAES-ISAMS)/CLAES, for January 10, 1992, for CLAES 12.65-μm and ISAMS 12.11-μm data, for 32°S to 80°N latitude, for 100, 68, 46, 31, and 21 hPa.

tion, when the theoretical ratio of extinction is factored into the comparisons.

Figures 12 and 13 illustrate the longitudinal cross sections of extinction at only two latitudes. To obtain statistics of the comparisons for the CLAES and ISAMS data, for a range of latitudes, RMS and average percent differences for the data sets were calculated using the mapped data in the following manner. The percent differences were first calculated at each 4° bin in latitude and each 5° bin in longitude (with 73 bins along a latitude line). Zonal sums of the percent differences, divided by 73, formed the "average percent difference" at each latitude. The square root of the zonal average of the squares of the percent differences formed the "RMS percent difference" at each latitude. Figures 14 and 15 present the results of the statistical calculations. Figure 14a displays the RMS percent differences for April 22, 1992, and Figure 14b presents the zonal average percent differences for the same days. If the differences between CLAES and ISAMS were totally random, then the averages presented in Figure 14b would meander about zero. Instead, the zonal averages are between 0 and 30% for pressure levels at 68, 46, 31, and 21 hPa. The nonzero average percent differences indicate systematic differences between the CLAES and the ISAMS extinctions. The RMS and average curves at 100 hPa indicate that the two instruments report very different extinction values in the equatorial latitudes, i.e., latitudes where the largest Mount Pinatubo aerosol extinction values are observed. The latitudinal structure in the graphs (excluding the 100-hPa curves) shows that the average and RMS percent differences become larger in the polar regions.

Figures 15a and 15b present the RMS and average percent difference statistics for January 10, 1992, for CLAES 12.65-μm and ISAMS 12.11-μm mapped data. The largest differences are again noticeable at the 100-hPa level. At the other pressure levels the RMS and average percent differences range between 10 and 60% and between -10 and 60%, respectively. For January 10, 1992, there is noticeable latitudinal structure in the CLAES-ISAMS differences, with the differences being largest at the higher northern latitudes.

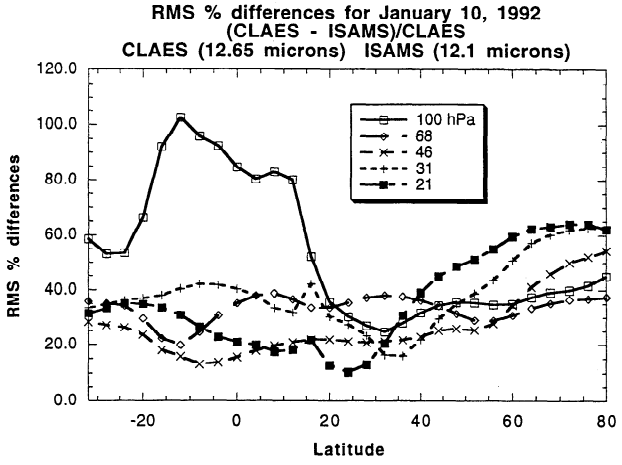

Figure 15a. RMS percent differences, 100x(CLAES-ISAMS)/CLAES, for January 10, 1992, for CLAES 12.65-μm and ISAMS 12.11-μm data, for 32°S to 80°N latitude, for 100, 68, 46, 31, and 21 hPa.

6. Conclusions

The comparisons of CLAES data with correlative measurements reveal a fairly consistent pattern. The 12.65-μm extinction is larger than that at 12.82 μm, which is contrary to expectation for sulfuric acid droplets. The differences between the data at these two wavelengths is of the order of 30%. For several of the comparisons both the 12.65- and the 12.82-μm extinctions are

Table 14. Empirical CLAES Aerosol rss Percent Accuracies

Wavelength, μm	Wavenumber, cm^{-1}	Pressure, hPa				
		21	31	46	68	100
12.82	780	36	33	34	34	34
12.65	790	36	33	33	34	34
11.90	840	38	36	35	35	35
11.36	880	43	41	38	37	43
10.83	925	39	35	37	37	37
7.95	1257	41	34	34	35	35
6.23	1605	56	35	34	34	117

Values are based upon precisions from Table 9 and empirical biases and offsets from Table 13.

larger than expectation, while the 10.83-μm extinction is smaller than expectation. CLAES extinction agrees closest to the correlative measurements at 46 hPa. At pressures less than 46 hPa and at 100 hPa the CLAES extinctions generally become larger than the transformed balloonsonde and SAGE II correlative measurements.

The conclusions in the preceding paragraph are problematic, however, since the utilization of the correlative measurements is difficult. A primary difficulty is due to uncertainties in the indices of refraction of sulfuric acid droplets. Accurate room temperature indices are needed to resolve the differences between the *Palmer and Williams* [1975] and *Remsberg et al.* [1974] tabulations, and accurate cold temperature indices are needed to improve upon the comparisons between observation and theory. A second issue is that the UARS extinction from CLAES, ISAMS, and HALOE all diverge away from the balloonsonde measurements at low-pressure levels. The CLAES and ISAMS data in Figure 12c agree to within 30% between 10 and 100 hPa, whereas the comparisons with correlative measurements in Figures 5 and 7 diverge at low and high pressures.

While several of the orbit-to-orbit precisions in Table 9 are below 10%, many of the values are between 10 and 25%. These precisions are larger than those cited in Tables 6 and 7. While the systematic errors in Tables 4 and 5 are of the order of 10%, a bias of 30% is apparent from the data (based upon differences in extinction at 12.82 and 12.65 μm). Future work needs to explain the 30% bias. The bias is surprising since the radiometric terms in Tables 4 and 5 are consistent with the known statistics of the temperature retrieval. As discussed by *Gille et al.* [this issue] in this validation issue, the CLAES temperature precisions are between 1 and 2°K, and a comparison of CLAES temperature data with NMC and UKMO analyses show general agreement to within 2–3 K.

On the basis of the orbit-to-orbit precisions of Table 9 and the biases and offsets of Table 13, Table 14 presents empirical accuracies. Most of the rss accuracies are between 33 and 43%. These are representative values. Latitudinal effects, such as the increase in the RMS and average differences between CLAES and ISAMS data (see Figures 13 and 14), are not reflected in this table. Note that error bars (quality indicators) are included with the archived CLAES data, and these reflect changes in instrument noise characteristics, which also are not reflected in Table 14.

Acknowledgments. Research at NCAR is supported by the NASA UARS program under contract S-10782-C. The National Center for Atmospheric Research is sponsored by the National Science Foundation. Work at the Lockheed Palo Alto Research Laboratory is supported by NASA under contract NAS5-27752. The ISAMS experiment is supported by the U.K. Science and Engineering Research Council and the National Environmental Research Council. The HALOE experiment is supported by NASA. The MLS experiment is supported by NASA, and the U.K. Science and Engineering Research Council and the British National Space Center, for work performed at the Jet Propulsion Laboratory and work conducted at the Rutherford Appleton Laboratory, Heriot-Watt University, and at Edinburgh University. Particle size distribution measurements by Terry Deshler are supported by NASA. Appreciation is extended to Curtis Rinsland of NASA Langley, who kindly forwarded the ATMOS data.

References

Cantrell, C. A., J. A. Davidson, A. H. McDaniel, R. E. Shetter, and J. G. Calvert, Infrared absorption cross sections for N_2O_5, *Chem. Phys. Lett.*, *148*, 358–363, 1988.

Deshler, T., B. J. Johnson, and W. R. Rozier, Balloonborne measurements of Pinatubo aerosol during 1991 and 1992 at 41°N: Vertical profiles, size distributions, and volatility, *Geophys. Res. Lett.*, *20*, 1435–1438, 1993.

Edwards, D. P., GENLN2: A general line-by-line atmospheric transmittance and radiance model, *NCAR/TN-367+STR*, Nat. Cent. for Atmos. Res., Boulder, Co., 1992.

Gille, J. C., et al., Accuracy and precision of Cryogenic Limb Array Etalon Spectrometer (CLAES) temperature retrievals, *J. Geophys. Res.*, this issue.

Grainger, R. G., A. Lambert, F. W. Taylor, J. J. Remedios, C. D. Rodgers, and M. Corney, Infrared absorption of volcanic stratospheric aerosols observed by ISAMS, *Geophys. Res. Lett.*, *20*, 1283–1286, 1993.

Hays, P. B., V. J. Abreu, M. E. Dobbs, D. A. Gell, H. J. Grassl, and W. R. Skinner, The High-Resolution Doppler Imager on the Upper Atmosphere Research Satellite, *J. Geophys. Res.*, *98*, 10,713–10,723, 1993.

Hervig, M. E., J. M. Russell III, L. L. Gordley, J. H. Park, and S. R. Drayson, Observations of aerosol by the HALOE experiment onboard UARS: A preliminary validation, *Geophys. Res. Lett.*, *20*, 1291–1294, 1993.

Kumer, J. B., et al., Comparison of correlative data with nitric acid version 7 from the Cryogenic Limb Array Etalon Spectrometer instrument deployed on the Upper Atmosphere Research Satellite, *J. Geophys. Res.*, this issue.

Lambert, A., R. G. Grainger, J. J. Remedios, C. D. Rodgers, M. Corney, and F. W. Taylor, Measurements of the evolution of the Mount Pinatubo aerosol cloud by ISAMS, *Geophys. Res. Lett.*, *20*, 1287–1290, 1993.

Lambert, A., R. G. Grainger, J. J. Remedios, W. J. Reburn, C. D. Rodgers, F. W. Taylor, J. L. Mergenthaler, J. B. Kumer, S. T. Massie, and T. Deshler, Validation of aerosol measurements by the Improved Stratospheric and Mesospheric Sounder, *J. Geophys. Res.*, this issue.

Marshall, B. T., L. L. Gordley, and D. A. Chu, BANDPAK: Algorithms for modelling broadbrand transmittance and radiance, *J. Quant. Spectrosc. Radiat. Transfer*, *52*, 563–580, 1994.

Massie, S. T., P. L. Bailey, J. C. Gille, E. C. Lee, J. L. Mergenthaler, A. E. Roche, J. B. Kumer, E. F. Fishbein, J. W. Waters, and W. A. Lahoz, Spectral signatures of Polar Stratospheric Clouds and sulfate aerosol, *J. Atmos. Sci.*, *51*, 3027–3044, 1994.

McCormick, M. P., and R. E. Vega, SAGE II measurements of early Pinatubo aerosols, *Geophys. Res. Lett.*, *19*, 155–158, 1992.

McCormick, M. P., C. R. Trepte, and M. C. Pitts, Persistence of polar stratospheric clouds in the southern polar region, *J. Geophys. Res.*, *94*, 11,241–11,251, 1989.

Mergenthaler, J. L., J. B. Kumer, and A. E. Roche, CLAES south-looking aerosol observations for 1992, *Geophys. Res. Lett.*, *20*, 1295–1298, 1993.

Mergenthaler, et al., Validation of Cryogenic Limb Array Etalon Spectrometer $ClONO_2$ measurements, *J. Geophys. Res.*, this issue.

Orlando, J. J., G. S. Tyndall, K. E. Nickerson, and J. G. Calvert, The temperature dependence of collision-induced absorption by oxygen near 6 μm, *J. Geophys. Res.*, *96*, 20,755–20,760, 1991.

Palmer, K. F., and D. Williams, Optical constants of sulfuric acid; application to the clouds of Venus?, *Appl. Opt.*, *14*, 208–219, 1975.

Read, W. G., L. Froidevaux, and J. W. Waters, Microwave limb sounder measurement of stratospheric SO_2 from the Mount Pinatubo volcano, *Geophys. Res. Lett.*, *20*, 1299–1302, 1993.

Remsberg, E. E., D. Lavery, and B. Crawford, Optical constants for sulfuric and nitric acids, *J. Chem. Eng. Data*, *19*, 263–265, 1974.

Rinsland, C. P., G. K. Yue, M. R. Gunson, R. Zander, and M. C. Abrams, Mid-infrared extinction by sulfate aerosols from the Mount Pinatubo eruption, *J. Quant. Radiat. Transfer*, *52*, 241–252, 1994.

Roche, A. E., J. B. Kumer, J. L. Mergenthaler, G. A. Ely, W. G. Uplinger, J. F. Potter, T. C. James, and L. W. Sterritt, The Cryogenic Limb Array Etalon Spectrometer on UARS: Experiment description and performance, *J. Geophys., Res.*, *98*, 10,763–10,775, 1993.

Roche, A. E., J. B. Kumer, J. L. Mergenthaler, R. W. Nightingale, W. G. Uplinger, G. A. Ely, J. F. Potter, D. J. Wuebbles, P. S. Connell, and D. E. Kinnison, Observations of lower-stratospheric $ClONO_2$, HNO_3, and aerosol by the UARS CLAES experiment between January 1992 and April 1993, *J. Atmos. Sci.*, *51*, 2877–2902, 1994.

Roche, A. E., et al., Validation of CH_4 and N_2O measurements by the Cryogenic Limb Array Etalon Spectrometer instrument on the Upper Atmosphere Research Satellite, *J. Geophys. Res.*, this issue.

Rodgers, C., Retrieval of atmospheric temperature and composition from remote measurements of thermal radiation, *Rev. Geophys.*, *14*, 609–624, 1975.

Russell, P. B., and M. P. McCormick, SAGE II aerosol data validation and initial data use: An introduction and overview, *J. Geophys., Res.*, *94*, 8335–8338, 1989.

Steele, H. M., and P. Hamill, Effects of temperature and humidity on the growth and optical properties of sulfuric acid-water droplets in the stratosphere, *J. Aerosol Sci., 12*, 517–528, 1981.

Taylor, F. W., A. Lambert, R. G. Grainger, C. D. Rodgers, and J. J. Remedios, Properties of northern hemisphere polar stratospheric clouds and volcanic aerosol in 1991/92 from UARS/ISAMS satellite measurements, *J. Atmos. Sci., 51*, 3019–3026, 1994.

Yue, G. K., M. P. McCormick, and W. P. Chu, Retrieval of composition and size distribution of stratospheric aerosols with the SAGE II satellite experiment, *J. Atmos. Oceanic Technol., 3*, 371–380, 1986.

World Meteorological Orgainzation (WMO), *Scientific Assessment of Ozone Depletion: 1991*, Geneva, 1991.

P. L. Bailey, C. P. Cavanaugh, C. A. Craig, J. C. Gille, L. V. Lyjak, S. T. Massie (corresponding author), National Center for Atmospheric Research, P. O. Box 3000, Boulder, CO 80307.

T. Deshler and E. Hervig, University of Wyoming, Laramie, WY 82071.

E. F. Fishbein and J. W. Waters, Jet Propulsion Laboratory, California Institute of Technology, Pasadena, CA 91109.

R. G. Grainger, A. Lambert, C. D. Rodgers, and F. W. Taylor, Atmospheric, Oceanic and Planetary Physics, Department of Physics, Clarendon Laboratory, Parks Road, Oxford, OX1 3PU, England.

J. B. Kumer, J. L. Mergenthaler, and A. E. Roche, Lockheed Palo Alto Research Laboratory, Palo Alto, CA 94304.

W. A. Lahoz, University of Reading, Reading, England.

J. M. Russell III and J. H. Park, NASA Langley Research Center, Hampton, VA 23666.

(Received December 19, 1994; revised July 22, 1995; accepted September 9, 1995.)